Charged Particle Irradiation for High-Performance Battery Anode

Jaewoo Lee, Jun Heo, Seunguk Cheon, Sung Oh Cho*
Dept. of Nucelar & Quantum Engineering, Korea Advanced Institute of Science & Technology, Daejeon, Republic of Korea, 34141
**Corresponding author: socho@kaist.ac.kr*

***Keywords :** charged particle irradiation, anode materials, lithium-ion batteries

1. Introduction

Energetic charged particles are able to induce significant damage to materials with multiple atomic displacements. The irradiation damage leads to changes in various features such as electronic and chemical properties. Many kinds of thin films have been studied to enhance their specific characteristics using charged particle irradiation [1,2]. Recently, electrochemical applications have been greatly promising in terms of energy storage and conversion. One of ongoing interest is electrode materials for secondary batteries and the electrode materials are considerably related to the battery performance.

Current commercialized electrode materials are limited to their low theoretical capacity, and particularly, the anodic part possesses great potential to realize larger capacity. There are a lot of candidates as alternatives to commercial graphite anode materials, however, they generally show poor cycle stability despite of their high capacity. In addition, the integrity of anode materials under fast charging and discharging should be also considered.

This study aims to figure out the irradiation effects on structural variation and electrochemical performance of anode materials. Lithium-ion batteries are targeted for the investigation, which is the most popular type. We adopt tin oxyhydroxide nanoparticles as active materials due to their high theoretical capacity [3]. Charged particle irradiation is highly applicable to miscellaneous electrochemical fields and versatile to improve the performance of functional thin films.

2. Experimental Section

2.1 Electrode Fabrication

Tin oxyhydroxide ($Sn_6O_4(OH)_4$) nanoparticles were obtained via an electrochemical anodization method [4]. Electrode materials were synthesized by blending the nanoparticles with carbonaceous Super P conducting agent and polyvinylidene (PVDF) binder in *N*-methyl-2-pyrrolidone solvent at a weight ratio of 4:5:1. The resulting mixture was cast on 10 μm thickness copper foil with a loading level of ~0.5 mg/cm^2. The average thickness of electrode material was directly measured to be 10 μm. The prepared electrodes were roll-pressed by 30% at 75℃ and were dried in a vacuum at 80℃ for 20 h.

2.2 Charged Particle Irradiation

Electron irradiation was carried out using a 50 kV electron beam facility (Korea Advanced Institute of Science and Technology, Daejeon, Korea). Electron energy was 50 keV and electrons were incident to the perpendicular to electrode surface. Absorbed dose by electron irradiation was calculated using the Monte Carlo N-Particle Transport Extended (MCNP6X) code. Gaseous ion irradiation was employed using a 200 kV gaseous ion beam facility (Korea Multi-purpose Accelerator Complex, Gyeongju, Korea). Helium, argon, and nitrogen ions were designated and the incident energy was 120 keV with a direction perpendicular to the electrode surface. Damage in displacement per atom (dpa) was calculated using the Stopping and Range of Ions in Matter (SRIM-2013) software. All irradiation processes were performed in a vacuum at room temperature.

2.3 Characterization

Field-emission scanning electron microscopy (FESEM) was utilized to observe the electrode surface. Nitrogen adsorption of the electrode material was measured at 77 K using a surface area and pore size analyzer. Electron spin resonance (ESR) spectroscopy, a high-resolution Raman/PL system with a 514 nm laser, X-ray photoelectron spectroscopy (XPS) with Al Kα radiation, and Fourier transform infrared (FTIR) spectroscopy were conducted to analyze the chemical structure of the electrode material.

2.4 Electrochemical Measurements

CR2032-type coin cells were assembled with the prepared electrodes (15 mm in diameter) as the working electrode and 300 μm thick lithium foil (16 mm in diameter) as the counter electrode. 16 μm thickness polyethylene (19 mm in diameter) was used as the separator. 1 mol/L lithium hexafluorophosphate dissolved in ethylene carbonate, dimethyl carbonate, and ethyl methyl carbonate (1:1:1 v/v) with 3 wt% fluoroethylene carbonate additive was used as an

electrolyte solution. Galvanostatic charging-discharging was applied in a potential range between 0.005 and 3 V (vs. Li/Li^+). The first cycle was at a current rate of 0.1 C (1 C = 838.05 mAh/g) and the remaining cycles were at a current rate of 0.5 C. Electrochemical impedance spectroscopy (EIS) was conducted in a frequency range between 100 kHz and 10 mHz using a 10 mV amplitude alternating current. All measurements were performed at room temperature.

3. Results and Discussion

3.1. Surface Properties

The surface morphology of the electrode before irradiating charged particles is shown in Fig. 1a. The surface is highly porous with homogeneously distributed electrode materials. The calculated Brunauer-Emmett-Teller specific surface area is 167.2 m^2/g from the N_2 adsorption isotherm in Fig. 1b, which confirms wide reactive area.

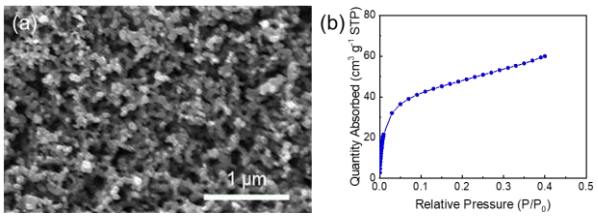

Fig. 1. (a) FESEM surface image and (b) N_2 adsorption isotherm of the electrode material before irradiation.

3.2. Charging-Discharging Performance

The electrodes were subjected to irradiation with four types of charged particles and the cycle performances of irradiated electrodes for each particle were evaluated. Fig. 2a shows the capacity and coulombic efficiency of e^--irradiated electrodes for each cycle. The pristine electrode exhibits an initial capacity of 2287.7 mAh/g but the capacity gradually decreases as the cycle proceeds. A rapid capacity loss is observed after 15 cycles and the capacity after 150 cycles is only 530.3 mAh/g. For the e^--irradiated electrodes, the initial capacity is similar to that of the pristine electrode, however, the capacity is preserved for longer cycles regardless of absorbed dose. The cycle stability is greatly related to the binder and e^- irradiation allows the PVDF binder to be crosslinked by dehydrofluorination [5]. The crosslinking enhances the mechanical strength and thermal property of PVDF binder, resulting in better cycle life. The overall coulombic efficiency of all electrodes is ~97%. In the case of He^+-irradiated electrodes given in Fig. 2b, the initial capacity is higher as the He^+ fluence increases. The capacity rise is ascribed to more reactions with lithium ions from defect sites induced by He^+ irradiation [6]. Nevertheless, the increased capacity suffers from severe fading for 100 cycles, which may result from the destruction of binder components. Average coulombic efficiency is also calculated to be ~97%. Similar behavior is seen in the case of Ar^+-irradiated electrodes shown in Fig. 2c. The Ar^+-irradiated electrodes have a larger capacity than the pristine electrode, particularly, the capacity is retained until 50 cycles at low-fluence irradiation. It is also attributed to the crosslinking of binder by low irradiation damages. The electrode with the highest Ar^+ fluence shows poor cycle life, which means considerable decomposition of binder happens from irradiation. All electrodes have an average coulombic efficiency of ~97%. Instead of inert gas ion, electrode performance after N^+ irradiation is presented in Fig. 2d. Larger initial capacity is attained when the fluence is higher and it is 2879.1 mAh/g at 1×10^{17} N^+/cm^2. N^+ irradiation helps the electrode materials to generate diverse defects, allowing additional reaction regions [6]. Interestingly, all of the irradiated electrodes exhibit significantly stable cycle characteristics, unlike the cases of inert gas ions. Energetic inert gas ions induce both crosslinking and decomposition of PVDF, where PVDF is not able to play a role as a binder after high-fluence irradiation. Conversely, N^+ particles rarely decompose PVDF due to combinable N atoms with delocalized electrons, preserving the structure of PVDF by forming C-N bonds. Therefore, crosslinked and N-doped binder boasts its high mechanical property and electrical conductivity, resulting in excellent cycle performance of electrodes. The N^+-irradiated electrode at the highest fluence exhibits a high capacity of 1403.9 mAh/g even after 150 cycles, which is ~3.8 times larger than the theoretical capacity of graphite. Likewise, all of N^+-irradiated electrodes have ~97% in coulombic efficiency on average.

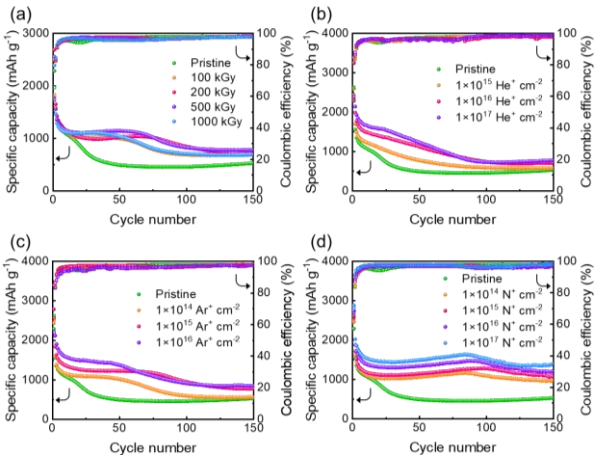

Fig. 2. Cycle performance of the electrodes irradiated with (a) e^- particles, (b) He^+ particles, (c) Ar^+ particles, and (d) N^+ particles.

Irradiation damage induced by heavy charged particles was calculated to ascertain the variation in cycle performance. Fig. 3a presents dpa distribution depending on the depth of electrode material irradiated

with He^+ at a fluence of 1×10^{17} He^+/cm^2. A Bragg peak is observed but it is expected that dpa would be more widely distributed in practice because of the highly porous structure. The theoretical density of the electrode material is 2.22 g/cm^3 but the actual density is calculated to be 0.5 g/cm^2 from the loading level and thickness due to substantial empty sites. Accordingly, an endpoint of dpa may be much deeper, which would cover the whole thickness of the anode materials with the identical peak position. The dpa distribution would have better homogeneity with lessened value because of the widened depth range, where the area under the curve is the same. In the case of Ar^+ irradiation at a fluence of 1×10^{16} Ar^+/cm^2 in Fig. 3b, the total damage is slightly larger than that of the He^+ irradiation case. Although the damage is higher at Ar^+ irradiation, the initial capacity rise is somewhat lower because there are some intact regions due to the shorter penetration depth. Therefore, lithium-ion diffusion is limited, leading to less reaction. Damage distribution of N^+ irradiation at a fluence of 1×10^{17} N^+/cm^2 is shown in Fig. 3c. The total damage is very large, however, considerable damage would be transferred to the binder so actual damage to active materials may be small. Additionally, inert gas ions produce only vacancy defects but there are different kinds of defects consisting N component, which is not capable to exhibit capacity. The approximate real penetration depth of N^+ ions is 8.89 μm, close to the thickness of the electrode material. Consequently, less increase in initial capacity is achieved at N^+ irradiation compared with He^+ irradiation.

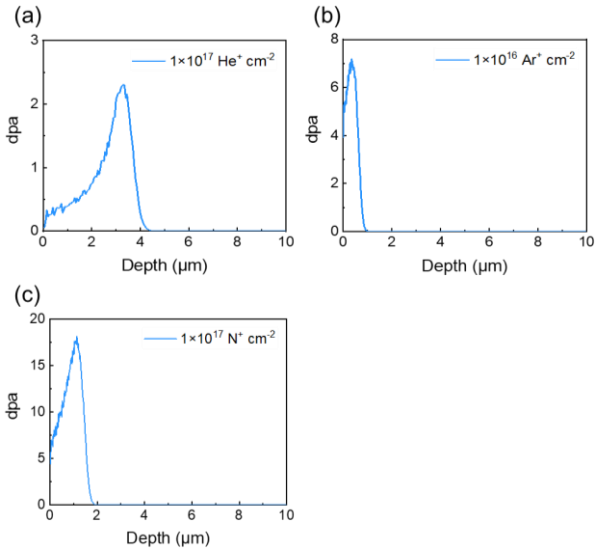

Fig. 3. Calculated damage of the electrodes irradiated with (a) He^+ particles, (b) Ar^+ particles, and (c) N^+ particles.

3.3 Structural Effects

Irradiation effects were confirmed by chemical investigations and Fig. 4a shows ESR spectra of N^+-irradiated electrodes. An intense signal is observed at g = 2.002 after N^+ irradiation, which corresponds to the creation of surface defect and oxygen vacancy (VO). The signal becomes greater as fluence increases and N^+ irradiation induces a large number of defects. Raman spectra are also presented in Fig. 4b. With increasing fluence, the G band shifts to a lower value, and the intensity ratio of the D band to the G band (I_D/I_G) gets smaller. It suggests that plentiful defects are generated in the carbonaceous conducting agent after irradiation [7]. The N^+-induced defects would act as the active material for electrochemical reactions, resulting in more capacity. XPS C 1s spectra in Fig. 4c,d also demonstrate the defect creation in conducting agent. The sp^2 C-C bonds get smaller after N^+ irradiation, and simultaneously, sp^3 C-C bonds grow. Various chemical bonds between C and N are also observed and C-F_2 bonds are diminished after irradiation. A significant decrease in C-F_2 bonds insists that the binder is damaged by irradiation. Generation of O-N groups and more VO content after irradiation are seen by comparing XPS O 1s spectra in Fig. 4e,f.

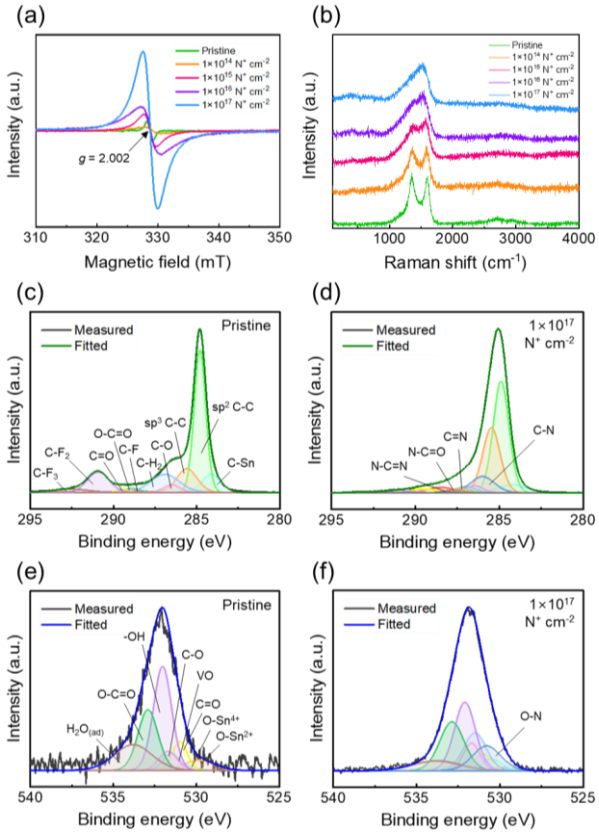

Fig. 4. (a) ESR, (b) Raman, (d) XPS C 1s, and (f) XPS O 1s spectra of the electrodes irradiated with N^+ particles. (c) XPS C 1s and (e) XPS O 1s spectra of the pristine electrode.

Fig. 5a shows FTIR spectra at each N^+ fluence. In enlarged spectra, no PVDF-related peaks are found after N^+ irradiation, supporting the damage to the binder. XPS F 1s spectra in Fig. 5b confirm the damage of the binder, where the peak intensity becomes weaker as fluence increases. The little PVDF-related peaks ascertain the crosslinking of the binder.

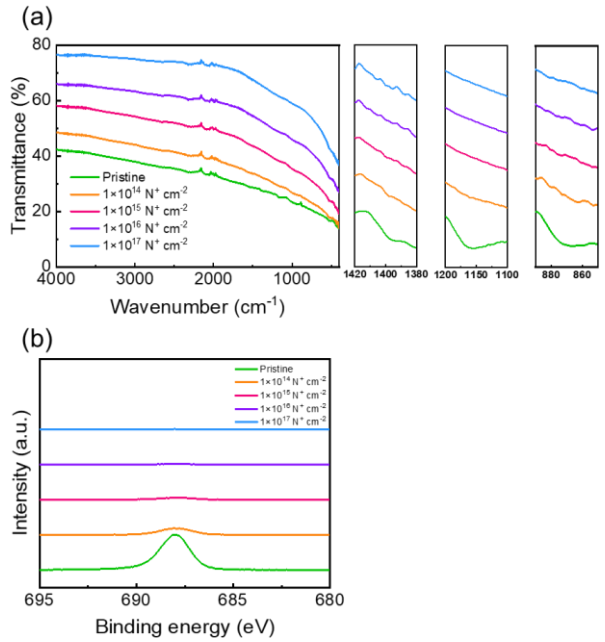

Fig. 5. (a) FTIR and (b) XPS F 1s spectra of the electrodes irradiated with N^+ particles.

3.4. Electrochemical Activities

Further electrochemical properties of N^+-irradiated electrodes were performed and Fig. 6a presents EIS spectra depending on N^+ fluence with an equivalent circuit (inset). Measured charge-transfer resistance (R_{ct}) is decreased at higher fluences, where R_{ct} is 205.1 and 99.5 Ω for pristine and 1×10^{16} N^+/cm^2 electrodes, respectively. Lower R_{ct} indicates better electrochemical behavior, allowing more capacity. The lithium-ion diffusion coefficient (D_{Li+}) is also estimated using linear fittings in Fig. 6b plotted from each EIS spectrum in low-frequency regions. A lower slope at higher fluence implies faster ion diffusion in the electrode material. The calculated D_{Li+} of the irradiated electrodes with 1×10^{16} N^+/cm^2 is 2.78×10^{-16} cm^2/s, which is 1.84 times quicker than that of the pristine electrode. Accordingly, N^+ irradiation to tin oxyhydroxide nanoparticle anode materials facilitates lithium-ion diffusion by rich active defects and enhances the structural stability of the binder, resulting in appreciable cycle performance.

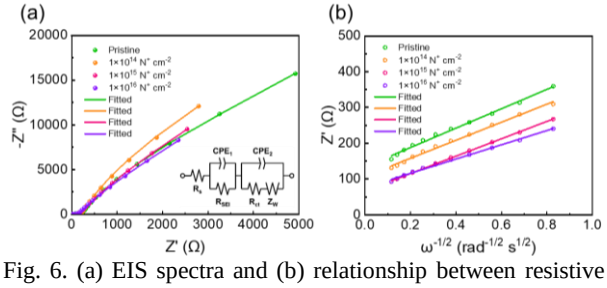

Fig. 6. (a) EIS spectra and (b) relationship between resistive impedance and frequency of the electrodes irradiated with N^+ particles

4. Conclusions

Cycle performances of charged-particle-irradiated tin oxyhydroxide nanoparticle anodes were compared. e^--irradiated electrodes showed better cycle life than the pristine electrode. Gaseous ion irradiation led larger initial capacity of electrodes but severe capacity fading was inevitable. Both significant increases in capacity and improved cycle stability were accomplished by irradiating N^+ ions to the electrode material, resulting from created reactive defects and mechanically enhanced binder, respectively. N^+-irradiated electrodes also exhibited efficient electrochemical properties so high-performance battery electrodes would be feasible.

ACKNOWLEDGEMENTS

This work was supported by the National Research Foundation of Korea (NRF) grant funded by the Korean government (MSIT) (No. 2019M2D2A1A0205817423) and was also supported by the Korea Technology & Information Promotion Agency for SMEs (TIPA) grant funded by the Korean government (MSS) (No. S3207719).

REFERENCES

[1] Y. Chen, S. Huang, X. Ji, K. Adepalli, K. Yin, X. Ling, X. Wang, J. Xue, M. Dresselhaus, J. Kong, and B. Yildiz, Tuning Electronic Structure of Single Layer MoS_2 through Defect and Interface Engineering, ACS Nano, Vol.12, pp.2569-2579, 2018.
[2] X. Xiang, Z. He, J. Rao, Z. Fan, X. Wang, and Y. Chen, Applications of Ion Beam Irradiation in Multifunctional Oxide Thin Films: A Review, ACS Applied Electronic Materials, Vol.3, pp.1031-1042, 2021.
[3] N. Spinner, L. Zhang, and W.E. Mustain, Investigation of metal oxide anode degradation in lithium-ion batteries *via* identical-location TEM, Journal of Materials Chemistry A, Vol.2, pp.1627-1630, 2014.
[4] J. Lee, N.E. Lee, S.Y. Lee, S. Cheon, and S.O. Cho, Defect-rich ultrafine amorphous tin oxyhydroxide nanoparticle anode for high-performance lithium-ion batteries, Materials Today Sustainability, Vol.22, p.100370, 2023.
[5] Y. Park, J.S. Park, S.-H. Baek, and J.H. Kim, Electron beam modification of anode materials for high-rate lithium ion batteries, Journal of Power Sources, Vol.296, pp.109-116, 2015.
[6] K.A. Smith, A.I. Savva, C. Deng, J.P. Wharry, S. Hwang, D. Su, Y. Wang, J. Gong, T. Xu, D.P. Butt, and H. Xiong, Effects of proton irradiation on structural and electrochemical charge storage properties of TiO_2 nanotube electrodes for lithium-ion batteries, Journal of Materials Chemistry A, Vol.5, pp.11815-11824, 2017.
[7] J. Robertson, Diamond-like amorphous carbon, Materials Science and Engineering: R: Reports, Vol.37, pp.129-281, 2002.